

Nonoriented Electrical Steels

FERNANDO JOSE GOMES LANDGRAF^{1,2}

1.—Escola Politécnica, Universidade de São Paulo and Instituto de Pesquisas Tecnológicas (IPT), 05508-901 São Paulo, SP, Brazil. 2.—e-mail: f.landgraf@usp.br

The physical origins of the magnetic properties of nonoriented electrical steels; its relations to microstructural features like grain size, nonmetallic inclusions, dislocation density distribution, crystallographic texture, and residual stresses; and its processing by cold rolling and annealing are overviewed, using quantitative relations whenever available.

Nonoriented electrical steels are the most economical choice of material used in electrical machines to transform electricity in movement, as in the electric car motors, or to transform movement into electricity, as in the wind mills generators, due to their capacity to amplify several thousand times the magnetic field generated by electric currents. They have been in use since the beginning of commercial electricity, around 1850. The name was coined in the 1930s to differentiate them from the newly invented grain-oriented electrical steels, a class of steels with 3% silicon in which a very strong (110)[001] crystallographic texture is developed by abnormal grain growth.

The world market for nonoriented electrical steels reached 14 million tons per year¹ in 2008, keeping its niche position as 1% of total steel production. It is reasonable to admit that its growth rate should follow the increase in electricity demand, which had a yearly average of 3.5% in the first decade of the 21st century, after a 2.5% average in the last decade of the 20th century. New products for new applications are blooming, led by their use in wind generators and electric car motors.

No radical innovation was introduced since the last review paper about the subject in this magazine² in 1986: The dream of a science wish list of the 1980s, three tesla saturation magnetization material, is yet to be discovered. The processing steps to achieve the ideal crystallographic texture (100)[uvw] in steels for electrical motors application have not been developed; despite the success in the modeling of texture evolution in cold rolling,³ recrystallization texture still lacks a better understanding. The promise of significant cost reduction and better texture by strip casting has not reached mass production scale.⁴ The commercial introduction of 6.5%

silicon strips is a significant innovation of the period.⁵ Nevertheless, the ever present energy conservation effort⁶ led to significant incremental innovations that will be discussed.

The Materials Science Tetrahedron⁷ suggests that we look for the relations between its four vertices: performance, properties, processing, and microstructure. Materials scientists like to focus on the relationships between property and microstructure and between process and microstructure, but we need to start by discussing the relation between component performance and properties, magnetic properties. Taking an electric motor as the main application, its torque is proportional to the magnetic flux (the unit is weber, Wb) in the air gap between the stator and the rotor. The flux intensity is directly connected with the ability of the material to amplify the magnetic field, somewhat inappropriately called magnetic permeability. As the magnetization curve has an S shape, magnetic permeability is not constant, and for quality control purposes, it is specified at certain points of the curve. The properties expressed in the magnetization curve are magnetic induction (also known as flux density B, in units of weber [volt second] per square meter, known as tesla, T) and the magnetic field (H field, in ampere per meter). Permeability in electrical steels is addressed in two different ways: ASTM defines the relation between specified values of magnetic induction and the magnetic field needed to achieve it (as in magnetic permeability $\mu_{1.5} = 1.5/\mu_0 H$), while IEC specifies the magnetic induction to be achieved at a certain value of magnetic field (as in B_{50} , the induction obtained with $H = 50$ A/cm). Flux performance is so sensitive to the size of the air gap that small differences in magnetic permeability are accepted. On the other hand, the concern with

energy conservation makes ever more important the control of the electric power loss in alternating current applications.

The magnetic hysteresis curve is the source of most information for electrical steels used in alternating current applications. The area of the curve corresponds to the dissipated energy density per cycle (in Joule/m³). Considering the applied frequency, the energy loss per cycle can be translated into electric power loss, in watts. Power loss density is expressed in watts per kilogram. It is very sensitive to excitation frequency, as shown in Fig. 1 and to the maximum induction value. The motor designer has to optimize cost and performance: For constant magnetic flux, cost is decreased by a smaller active area of magnetic materials, but that can only be done by increasing flux density, which increases hysteresis area.

The magnetic behavior of the steels is associated with the changes in the ferromagnetic domain structure as magnetization is changed. A magnetic domain is a volume of the material where all the iron atoms point their magnetic moments, which originate in their unpaired electron spins, in one of the $\langle 100 \rangle$ directions. Quantum mechanics behavior of the 3d electrons is the source of the exchange energy that explains and quantifies the parallelism. The parallelism of the atomic moments is challenged by thermal vibration, and above the Curie temperature, ferromagnetism does not exist. The exchange energy constant is in the order of 400 MJ/m³. In the border between neighboring domains, there exists a 0.2- μm -thick magnetic domain wall,⁸ where the magnetic moment makes a transition between the neighbor's directions. Between anti-parallel domains, the 180° domain wall is twice as thick as the 90° domain wall between orthogonal domains. The energy density of the domain wall is in the order of 1.5 mJ/m², decreasing slightly with silicon content. Magnetic domains can be seen in the surface of a magnetic material using polarized light, whose polarization plane is changed by an interaction with the magnetic polarization of the domain. Figure 2 shows the domain structure⁹ that can be

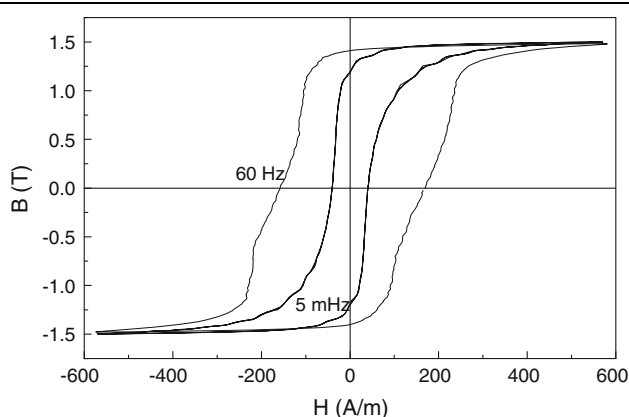


Fig. 1. Hysteresis curves at 60 Hz and quasi-static conditions.

observed in two neighboring grains separated by the curved grain boundary in the center. On the left side, one sees big dark and gray domains. On the right side, two big domains are seen with many small triangles of opposite color inside them. The domain structure on the left is typical to what is observed on a $\{100\}$ surface, while the structure on the right can be observed on a $\{110\}$ surface. One can see the continuity of domain walls when crossing from one grain to the other, even though directions change: The north pole of a domain must be facing the south pole of a neighboring domain, to minimize magnetostatic energy.

When an external magnetic field is applied, there is a buildup of magnetostatic energy in each domain. The accumulated energy density is given by the scalar product of the external field and the magnetic polarization inside the domain, whose value is that of the material's magnetic polarization saturation. Energy density is at minimum when the two vectors are parallel. As the external field is increased, magnetostatic energy can be minimized by the decrease in volume of the magnetic domains that are less well oriented. The vectorial sum of all the atomic magnetic moments of the material, per unit volume, gives the value of the magnetic polarization achieved by exposing the material to that field intensity. The change in domain volume happens by the movement of the domain wall. Domain wall movement is a mechanism of energy dissipation, as the local magnetization change will create an electrical potential due to Faraday's law ($V \propto dB/dt$), that will induce an electrical current flow that dissipates heat, according to Joule's law ($P = RI^2$). Energy is dissipated even in a quasi-static measurement of hysteresis, when magnetic field is changed by very low frequency. Domain wall movement is not infinitely slow even in that circumstance: Walls get pinned by magnetization discontinuities

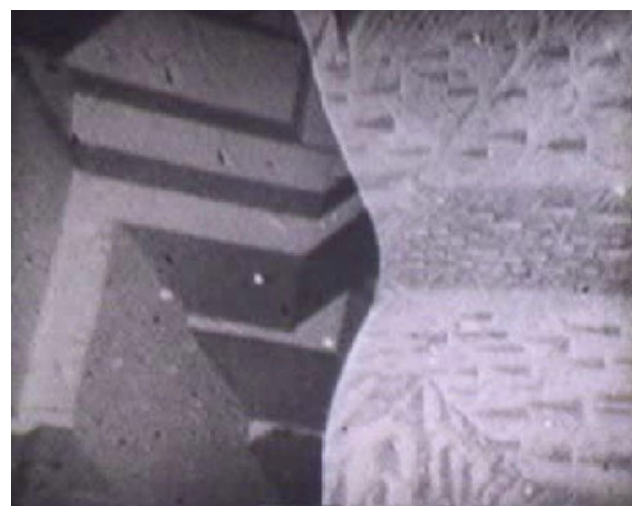


Fig. 2. Magnetic domain structure in electrical steel, as seen by Kerr effect.⁹

such as nonmetallic inclusions, grain boundaries, surface roughness, and dislocation walls until further increase in the external field builds enough magnetostatic energy to drive the walls out of these traps. They then move rapidly across the grains until being held by stronger pinning sites.

When the external field is large enough, the magnetic domains whose magnetization directions have components that are contrary to the applied field disappear, resting only domains with the three other $\langle 100 \rangle$ directions. A further increase of the external field will induce magnetic domain rotation. Due to quantum mechanics reasons associated with electron spin-orbit coupling, the unpaired electron spin direction spontaneously lies in one of the $\langle 100 \rangle$ directions of the iron crystals. Magnetocrystalline energy is accumulated when the atomic moment, to decrease the magnetostatic energy, is taken away from the direction in which it spontaneously lies. It is described by Akulov's equation, where α_i is the cosine of the angle between the applied field direction and each of the $\langle 100 \rangle$ crystal directions.

$$E_{mc} = K_1(\alpha_1^2\alpha_2^2 + \alpha_2^2\alpha_3^2 + \alpha_3^2\alpha_1^2) + K_2\alpha_1^2\alpha_2^2\alpha_3^2 \quad (1)$$

In most modeling studies, only the first parcel is considered, so only K_1 is used. The magnetocrystalline energy constant K_1 is $48,000 \text{ J/m}^3$ and K_2 is $5,000 \text{ J/m}^3$ for pure iron.¹⁰ To reach the saturation value of magnetic polarization in iron, a magnetic field of more than $40,000 \text{ A/m}$ is needed. Silicon and aluminum content (in wt.%) affect the constant according to Eq. 2¹¹

$$K_1 = (4.8 - 0.42\%Si - 0.08\%Al) * 10^4 \text{ J/m}^3 \quad (2)$$

One can see a "knee" in the quasi-static hysteresis curve of Fig. 1. It shows that a polarization of $0.9T$ can be achieved with 150 A/m , in the first quadrant, but to reach $1.5T$, about 600 A/m is needed. In the magnetization of electrical steels, a polarization of $0.8T$ is usually attained by domain wall movement. Above that, domain rotation is the main magnetization mechanism. Domain rotation has no pinning, so it is a reversible mechanism, which is nondissipative when happening infinitely slow. Magnetic domain wall movement is not reversible, so it is dissipative. Also dissipative is the domain rotation and the domain wall creation¹² that happens in a domain nucleation event.

Mechanical stresses have significant effects on the hysteresis curves of electrical steels, due to the magnetostriction phenomenon: There is a 10^{-5} expansion of steel bodies in the direction of magnetization, and conversely, compression stress enlarge and shear hysteresis curves. This is due to the fact that iron is not truly body-centered cubic, but tetragonal, 10^{-5} longer in the direction of the magnetization of each domain.

The area of the hysteresis curve corresponds to the energy dissipated per cycle per unit volume. The product of induction, given in Vs/m^2 , and magnetic

field, given in A/m , is J/m^3 . Figure 1 shows that the energy dissipated per cycle increases with frequency. The magnetic power loss is the product of the hysteresis area and frequency, divided by mass density. The standard quality indicator of electrical steels is the magnetic power loss at a certain frequency and maximum induction, given in watts per kilogram and valid for a certain sheet thickness. The grades of nonoriented electrical steels, both at ASTM and IEC, are defined by a number that represents the maximum accepted power loss for a certain sheet thickness. For example, steel grade M400-65 in IEC standard (where 50 Hz and $1.5T$ are the reference frequency and maximum induction) indicates that maximum accepted power loss for that grade is 4.0 W/kg , for a 0.65-mm -thick sheet.

The energy efficiency of motors is related to the most investigated subject of electrical steels, the magnetic power loss, called core-loss by ASTM, and specific total losses by IEC. Most of the information about microstructure-property relations in electrical steel is based on the measurement of magnetic power losses in alternating excitation, using the well-established method of the Epstein frame.^{13,14} The single sheet tester is already normalized¹⁵ and shows comparable results to the Epstein frame tests. Both have the shortcoming of measuring the property in only one direction¹⁵ or averaging two directions,¹³ while the magnetic losses are significantly anisotropic (at least 30% difference between rolling and transverse directions) and motor or generator application excite the material in different directions and amplitudes according to the position inside the part. More comprehensive alternatives have been proposed¹⁶ but not yet accepted.

The modeling of total magnetic power loss in alternating excitation has been the subject for many approaches, mostly from the electrical engineering point of view.^{17,18} A standard approach is to separate it in three components, hysteresis (P_h), parasitic (P_p), and anomalous (P_a), which is also known as excess loss. Cullity criticized this approach¹⁹ by arguing that all energy dissipation comes from the microcurrents associated with domain wall movement, turning meaningless the eddy currents supposed in the parasitic component. Nevertheless, the effect of sheet thickness and material electrical resistivity is so well described by the hundred years old parasitic equation²⁰ that most researchers still assume the loss separation to be reasonable. The frequency dependence of each loss component is different, linear in hysteresis loss, squared in parasitic loss and $3/2$ in anomalous loss.²¹

$$P_T = P_h + P_p + P_a = \frac{A_h \times f}{d} + \frac{(\pi B f e)^2}{6 \rho d} + K_a \times f^{3/2} \quad (3)$$

The equation explicitly shows that maximum induction (B) has a strong influence on the parasitic component. B also affects both the hysteresis and

anomalous component. Charles Proteus Steinmetz, in a classic paper of 1892, showed²² that the hysteresis area (A_h) increases with $B^{1.6}$. That exponent is consistent up to 1.2T, but above hysteresis loss is higher than what it predicts. Bertotti's model assumes,²³ for anomalous loss, that K_a increases with $B^{1.5}$. Equation 3 shows that sheet thickness (e), which usually ranges from 0.65 to 0.35 mm, affects significantly the parasitic component. Experimental results indicate no effect on hysteresis component, as long as the grain size is not larger than half thickness. Its effect on the anomalous loss is still debatable.²⁴ Electrical resistivity (ρ) affects parasitic loss according to Eq. 3 but does not affect hysteresis component. Its effect on anomalous loss has been considered as proportional to $1/\sqrt{\rho}$ or $1/\rho$, according to different authors.^{21,24}

Several equations have been proposed for the effect of chemical composition on electrical resistivity,^{25,26} based on which Eq. 4 is developed. Plastic deformation effects are negligible at room temperature.

$$\begin{aligned} \rho(\mu\Omega\text{cm}) = & 10.7 + 3.4 * (\%Mn) + 17 * (\%P) \\ & + 14 * (\%Si) + 12 * (\%Al) + 8 * (\%Sn) \end{aligned} \quad (4)$$

Microstructure affects hysteresis loss strongly and anomalous loss weakly, with no effect on parasitic loss. To minimize hysteresis loss, electrical steels should maximize grain size, ideally single-phase materials, containing as little carbides, oxides, nitrides, and sulfides as possible; lowest possible crystallographic dislocation density; minimum applied and residual mechanical stresses; and a crystallographic texture that maximizes the frequency of grains with $\langle 100 \rangle$ directions parallel to the sheet surface. For motor applications, the ideal texture is $\{100\}\langle 0vw \rangle$.

Processing of electrical steels has an important impact on the total losses. Plastic deformation increases hysteresis loss and decreases excess losses, while annealing promotes grain size increase that decreases the first and increases the second, as seen in Fig. 3. The total losses of non-oriented electrical steels, at 1.5T and 60 Hz, range from 10 W/kg to 3 W/kg, in annealed condition, as stated by steel-makers catalogs.

As grain size and plastic deformation have such a large influence on losses, nonoriented electrical steels are grouped in two classes, based on the processing route, but depending on the application: semiprocessed (SP)^{27,28} and fully processed steels (FP).^{29,30} Fully processed steels are delivered in annealed condition, ready to be punched and used, usually with no further heat treatments. When part dimensions are small, the magnetic property deterioration by the plastic deformation and residual stresses induced by punching are so significant that a final stress relieving thermal treatment is necessary. Considering that need, semiprocessed steels

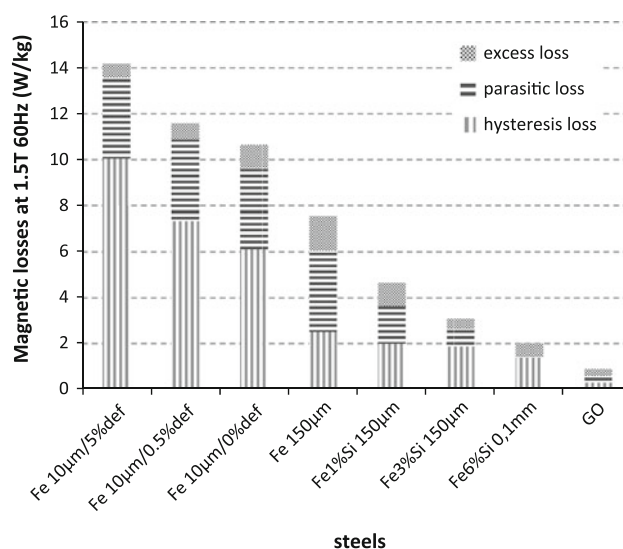


Fig. 3. Total loss and its components for steels with different silicon content and processing conditions, keeping constant maximum induction (1.5T), frequency (60 Hz), and thickness (0.5 mm), except for the grain-oriented material (0.35 mm).

are designed so that the stress relieving treatment promotes recrystallization³¹ that results in grain size increase. This is obtained when the steelmaker applies a small plastic deformation (between 3% and 8% thickness reduction) by cold rolling as the last stage before delivery. Several authors call the grain size increase that happens during the stress relief annealing treatment as “strain-induced abnormal grain growth,”^{32–34} although it follows all the rules of primary recrystallization.³⁵

The small amount of plastic deformation applied to nonalloyed semiprocessed steels may increase losses at 1.5T, 60 Hz to 15 W/kg, but after annealing, it drops to 7 W/kg, as dislocation density decreases and grain size increases. Some applications, like in automobile alternator stators produced by the helical winding process,^{36,37} demand plastic deformation to reach a high elastic ratio (the ratio between the values of yield stress/rupture stress). In those cases, energy efficiency is sacrificed for mechanical reasons.

Any alloying element (besides cobalt) will decrease saturation magnetic polarization, which results in lower magnetic permeability and higher hysteresis loss, unless a change in the crystallographic texture is simultaneously induced. Silicon and aluminum are the two major alloying elements of electrical steels due to their ability to decrease parasitic loss by increasing electrical resistivity. It was limited to 3.5% silicon since the 1920s, due to processing brittleness, until a breakthrough allowed it to each 6.5% Si in 1990.⁵ Manganese is also an alloying element, either in the small amounts needed to assure that all sulfur content is combined as manganese sulfide to avoid hot shortness during rolling, or in some conditions to improve crystallographic texture.³⁸ Due to its effect in increasing

electrical resistivity, phosphorus is used in contents around 0.1%, which are higher than those in steels for mechanical applications. Phosphorous also increases brittleness, which may have a contribution to the reduction of punching costs. Tin and antimony, in contents below 0.1%, are frequently added to electrical steels. Several reasons were proposed, as it decreases intergranular subsurface oxidation during annealing³⁹ and it may improve texture in some circumstances.⁴⁰

There is no clear statement of the effect of chemical composition on quasi-static hysteresis area. A slight effect may be expected as chemical composition changes domain wall energy value through its effect on anisotropy constant K_1 . Microstructural effects are much more important, as stated above. A first approach is that hysteresis area is an additive function of five microstructural parameters: grain size, texture, inclusion content, dislocation density distribution and stress distribution. Synergistic effects of these variables may have to be accounted for.

Grain size is controlled by grain growth, in the case of the fully processed steels, or by recrystallization in the case of the semiprocessed steels. Grain size is one of the most important variables, although its mechanism is not yet well established. Bozorth⁴¹ even considered that the relation between large grain size and low hysteresis loss was fortuitous, as he believed that the larger grain sizes were obtained by increasing annealing temperature, which decreased the average number of nonmetallic inclusions that supposedly was the true cause of hysteresis loss decrease. Other influential textbooks on magnetic materials also ignored the effect of grain size^{42–44} although an inverse proportionality was identified as early as the 1930s.^{25,45} Goodenough,⁴⁶ on the other hand, stated that the route to model hysteresis area passed through a better understanding of coercive field and its grain size dependence. Coercive force H_c is the magnetic field necessary to demagnetize the material, that is, to reach a zero value for induction, as seen in Fig. 1, and it determines the width of the hysteresis curve. A model for the relation between grain size and coercive force H_c was proposed by Mager⁴⁷ in 1952: When lowering the field from saturation, domain rotation increases demagnetizing fields at grain boundaries. The associated magnetostatic energy promotes the nucleation of inverse domain strings, as depicted in Fig. 4,⁴⁸ even before remanence. The string length is contained by the relation between domain wall energy (γ) increase and volumetric magnetostatic energy decrease. The string width is limited by the grain diameter (ℓ), as any width growth beyond the grain boundaries would imply in large magnetostatic energy increase, due to demagnetizing fields. A critical field had to be surpassed, in the second quadrant, to allow for the longitudinal growth of the strings, which is dependent on the grain diameter. This critical field is described by Eq. 5.

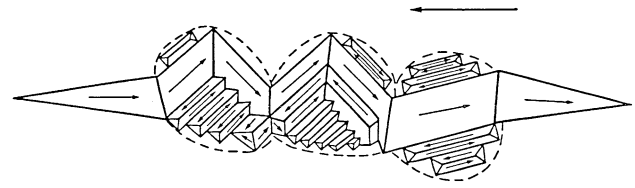


Fig. 4. Inverse domain strings existing at remanence, as proposed by Mager.⁴⁸ Its longitudinal growth is contained by the grain width until a critical field is surpassed.

$$H_c \cong 3 \frac{\gamma}{J_s * \ell} \quad (5)$$

There are disagreements on the exponent of the inverse dependence of hysteresis loss and grain size,^{25,49} but it is reasonable to assume it is proportional to $1/\ell$. Unfortunately, not enough data have been gathered to reach a universally accepted quantitative relation between hysteresis loss and grain size. Among the difficulties, an important one is that different grain size measurement techniques are used.⁵⁰ Maximum induction also has to be taken into account. The joint effect of grain size (in μm) and maximum induction on the hysteresis area A_h (in J/m^3) is described⁵¹ by Eq. 6.

$$A_h = 96 \times B_{\text{max}}^2 + \frac{3224 \times B_{\text{max}}^{1.4}}{\ell} \quad (6)$$

The final crystallographic texture is developed during the FP steels grain growth or the SP steels recrystallization stages of the final annealing, but it is influenced by previous actions in the hot rolling and cold-rolling stages. The most investigated mechanism for texture improvement is the nucleation of Goss grains in the shear bands of cold-rolled large grain size hot-bands.⁵² Some authors claim that the effect of tin and antimony in improving texture is associated with the promotion of a larger density of shear bands.⁴⁰ The approach of the effect of crystallographic texture on losses has changed significantly since 1986, although the principle that losses are decreased by increasing the amount of grains with directions $\langle 100 \rangle$ parallel to the sheet surface is maintained. Until then, several texture factors were tried in the texture-losses correlation, usually by the x-ray inverse pole intensity ratio I_{110}/I_{111} . The spread of the electron backscattered diffraction (EBSD) technique, complemented by texture representation by orientation distribution function (ODF), brought new options to describe the correlation. The qualitative approach of the effect of processing on texture still predominates,^{53–55} but two strategies to transform the orientation distribution into a single number to be correlated to magnetic losses have been proposed: the average magnetocrystalline anisotropy energy \bar{E}_{mc} accumulated when the material is saturated in the direction of the applied field⁵⁶ and A_θ the average angle⁵⁷ between the directions of the applied field and the closest $\langle 100 \rangle$ in each grain.

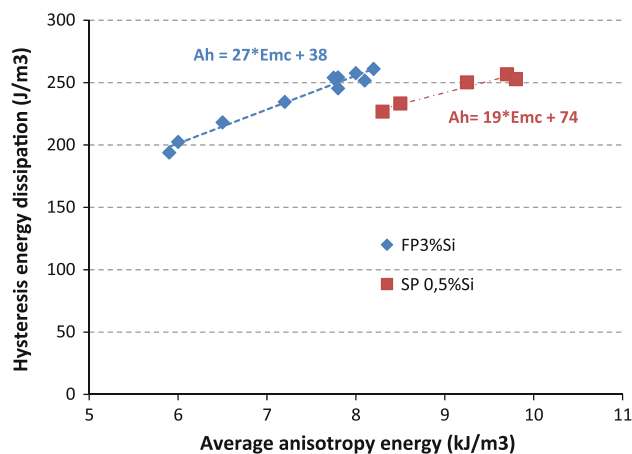


Fig. 5. Hysteresis loss per cycle of two steels, measured at different directions relative to the rolling direction, correlated to the average magnetocrystalline anisotropy energy calculated for each direction, based on texture measurements by EBSD.

The potential of those techniques can be foreseen in Fig. 5, where the hysteresis loss per cycle was measured in different directions relative to the rolling direction, and the average magnetocrystalline anisotropy energy \bar{E}_{mc} associated with each direction was calculated based on ODF data from x-ray measurements. The results for two different steels are shown, an FP 3%Si steel and a SP 0.5%Si steel. Interestingly, the comparison of the linear coefficients of the equations shown on that figure is consistent with the smaller grain size of the SP steel (70 μm , where FP steel has grain size of 140 μm).

The effect of nonmetallic inclusions is the least investigated in the literature. The 1986 review² had already shown that lowering either sulfur, oxygen, or nitrogen from 50 to 10 ppm would decrease losses at 1.5T, 50 Hz by 0.6 W/kg. Theory predicts that the worst inclusions are those with a particle size close to the domain wall thickness, that is, around 0.2 μm . Although that size range is not easy to produce good statistics for the number of inclusions per unit area on a polished surface, due to a weak contrast in scanning electron microscopy, very detailed results were shown for the effect of small additions of cerium to a 1.2% Si steel.⁵⁸ The article does not confirm the theoretical predictions and concludes that the positive effect of 30 ppm addition of cerium is more related to a combination of grain size and texture change. Several recent patents in this field insist on the positive effect of changing inclusions particle size on grain growth, inverting the above mentioned Bozorth's suggestion.

Plastic deformation causes a significant increase in hysteresis loss of electrical steels and so it must be avoided⁵⁹ or relieved by annealing.⁶⁰ The associated decrease of anomalous loss⁶¹ does not compensate it. Figure 6 shows that hysteresis energy dissipation nearly triples after 10% plastic deformation. Standard explanation relates it to the interaction between

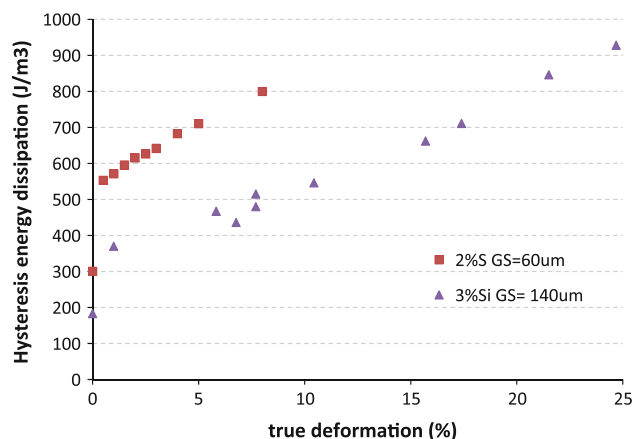


Fig. 6. Effect of plastic deformation on hysteresis loss per cycle.

domain walls and the dislocations produced by the deformation,⁶² leading to a proposal that hysteresis loss is proportional to the square root of the dislocation density. Some facts have to be considered to reach a better understanding of the relation between microstructure and properties in iron alloys.

1. Evidence of grain fragmentation at least above true deformation of 5%, where there is evidence of dislocations tangles that form dislocation cells inside each grain, each misoriented 2° to its neighbors,⁶³ plus dense dislocation walls that separate areas misoriented more than 20° as deformation increases
2. The magnetoelastic behavior of the compressed volumes associated with the microresidual stresses related to those dislocation structures^{64–66}
3. The surprising jump of hysteresis loss at very small deformation (less than 0.5%) represented in Fig. 6 for two different steels and noted in many other investigations^{67–69} is yet to be understood, as there is no similar mechanical behavior.

The introduction of 6.5%Si steels in very thin strips is a significant innovation in the nonoriented electrical steels field. It is commercially done by chemical vapor deposition of silicon onto a 3%Si strip, followed by a diffusion step.⁵ As its thickness can be taken to 0.1 mm and its resistivity reaches 82 $\mu\Omega\text{cm}$, its parasitic loss is negligible, so its total losses at 1.5T 60 Hz is around 2 W/kg, as shown in Fig. 3. Based on that route, it is possible to produce materials with a silicon content gradient, as there are advantages for that in some applications. A new route is being investigated, based on dipping a steel sheet in a hypereutectic silicon-aluminum bath where proeutectic silicon is deposited on the sheet surface,⁷⁰ followed by a diffusion annealing step.

The new applications to wind generators and electrical traction of cars have spurred developments to suit them. Wind generators, operating at low frequencies, permit the use of thicker sheets (1 mm) with higher B_{50} , while variable speed

motors for cars impose higher frequency harmonics that can be better dealt by thinner gauge materials (less than 0.3 mm). Hot- and cold-rolling processes had to be adapted to produce the required texture and grain size in those new thicknesses.

The strive for more precise design of a motor energy efficiency, in recent years, demands data about magnetic properties not only in sinusoidal alternating magnetic field excitation, but also under other wave form and or rotating field excitation.

Rotating power loss may be larger than the alternating excitation loss in some regions of electrical machines.⁷¹ Reflecting that situation, many researchers have devoted their time to this problem. According to ISI, the most cited paper about electrical steels, with 71 citations from 1993 to 2011, addresses this subject.⁷² The stage of the development is yet far from establishing relations between microstructure and that property, as no standard method of rotating magnetization measurement has been normalized.⁷³

Similar situation can be seen in the discussion of waveforms other than sinusoidal. The decreasing price of electronic power supplies has increased the use of pulse-width-modulated (switching or space-vector modulated sampling frequency in variable speed motors), presenting new challenges to the prediction of iron losses.^{74,75} Among several modeling strategies, Bertotti's proposal is a successful one, assuming the validity of power loss separation even under harmonic distortion in the flux density.⁷⁶

REFERENCES

1. C.-D. Wuppermann, *Proceedings of the 4th International Conference Magnetism and Metallurgy, WMM'10* (Freiberg, Germany, 2010), ed. TU-BAF.
2. G. Lyudkovsky, P.K. Rastogi, and M. Bala, *JOM* 38 (1), 18 (1986).
3. P. Van Houtte, S. Li, M. Seefeldt, and L. Delannay, *Int. J. Plast.* 21, 589 (2005).
4. H.T. Liu, Z.Y. Liu, Y. Sun, Y.Q. Qiu, and G.D. Wang, *Adv. Mater. Res.* 415, 947 (2012).
5. K. Okada, T. Yamaji, and K. Kasai, *ISIJ Int.* 36, 706 (1996).
6. A.J. Moses, *Scripta Mater.*, e-pub <http://dx.doi.org/10.1016/j.scriptamat.2012.02.027>.
7. L.H. Schwartz, *JOM* 62 (3), 34 (2010).
8. K.M. Podurets and S.S. Shilstein, *Phys. B* 297, 263 (2001).
9. G. Wolf, *Encyclopaedia Cinematographica* (Göttingen, Germany: Institut für den Wissenschaftlichen Film, 1971).
10. M.F. Littman, *IEEE Trans. Mag.* 7, 48 (1971).
11. R.C. Hall, *J. Appl. Phys.* 31, 1037 (1960).
12. M. Guyot and V. Cagan, *J. Magn. Magn. Mater.* 101, 256 (1991).
13. IEC 60404-2, *Magnetic Materials—Part 2: Methods of Measurement of the Magnetic Properties of Electrical Steel Sheet and Strip by Means of an Epstein Frame*, 1996.
14. ASTM A343/A343M-03, 2008, *Standard Test Method for Alternating-Current Magnetic Properties of Materials at Power Frequencies Using Wattmeter-Ammeter-Voltmeter Method and 25-cm Epstein Test Frame*, 2003.
15. IEC 60404-3, *Magnetic Materials—Part 3: Methods of Measurement of the Magnetic Properties of Magnetic Sheet and Strip by Means of a Single Sheet Tester*, 2010.
16. A. Honda, B. Fukuda, I. Oyama, and Y. Mine, *J. Mater. Eng.* 12, 41 (1990).
17. D.C. Jiles and D.L. Atherton, *J. Magn. Magn. Mater.* 61, 48 (1986).
18. S.E. Zirka, Y.I. Moroz, P. Marketos, and A.J. Moses, *IEEE Trans. Magn.* 46, 286 (2010).
19. B.D. Cullity, *Introduction to Magnetic Materials* (Reading, MA: Addison Wesley, 1972).
20. J.J. Thomson, *Electrician* 8, 599 (1892).
21. G. Bertotti, *IEEE Trans. Magn.* 24, 621 (1988).
22. C.P. Steinmetz, *Trans. AIEE* 9, 3 (1892).
23. M. LoBue, C. Sasso, V. Basso, F. Fiorillo, and G. Bertotti, *J. Magn. Magn. Mater.* 215, 124 (2000).
24. E.T. Stephenson, *J. Appl. Phys.* 57, 4226 (1985).
25. T.D. Yensen, *Trans. ASM* 797 (1939).
26. E.T. Stephenson and M.R. Amann, *Energy Efficient Electrical Steels*, Vol. 43 (Warrendale, PA: TMS-AIME, 1981).
27. IEC 60404-8-3, *Magnetic Materials—Part 8-3: Specifications for Individual Materials—Cold-Rolled Electrical Non-Alloyed Steel Sheet, and Strip Delivered in the Semi-Processed State*, 2008.
28. ASTM A683-05 *Standard Specification for Nonoriented Electrical Steels, Semiprocessed Types*, 2005.
29. IEC 60404-8-4, *Magnetic Materials—Part 8-4: Specifications for Individual Materials—Cold-Rolled Non-Oriented Electrical Steel Sheet and Strip Delivered in the Fully Processed State*, 2005.
30. ASTM A677-07 *Standard Specification for Nonoriented Electrical Steel Fully Processed Types*, 2007.
31. D. Stojakovic, R.D. Doherty, S.R. Kalidindi, and F.J.G. Landgraf, *Metall. Mater. Trans. A* 39, 1738 (2008).
32. G. Riontino, C. Antonione, L. Batezzati, and F. Marino, *J. Mater. Sci.* 14, 86 (1979).
33. J.A. Kowalik and A.R. Marder, *Scripta Metall.* 18, 305 (1984).
34. S.W. Cheong, E.J. Hilinski, and A.D. Rollett, *Metall. Mater. Trans. A* 34, 1321 (2003).
35. R.D. Doherty, D.A. Hugues, F.J. Humphreys, J.J. Jonas, D.J. Jensen, M.E. Kassner, W.E. King, T.R. Mcnelly, H.J. Mcqueen, and A.D. Rollett, *Mater. Sci. Eng. A* 238, 219 (1997).
36. R. Retana, A. Shendi, E. Rau, and R. Meyer, *Proceedings of the 3rd International Conference on Magnetism and Metallurgy, WMM'08* (Gent, Belgium, 2008), ed. TU-BAF.
37. M. Kawano, T. Fujiyama, and T. Aoki, *Kawasaki. Tech. Rep.* 48, 47 (2003).
38. P.K. Rastogi, *IEEE Trans. Magn.* 13, 1448 (1977).
39. G. Lyudkovsky, *IEEE Trans. Magn.* 22, 508 (1986).
40. M. Takashima, T. Obara, and T. Kan, *J. Mater. Eng. Perf.* 2, 249 (1993).
41. R.M. Bozorth, *Ferromagnetism* (New York: Van Nostrand, 1951).
42. S. Chikazumi, *Physics of Magnetism* (New York: John Wiley & Sons, 1964).
43. B.D. Cullity and C.D. Graham, *Introduction to Magnetic Materials*, 2nd ed. (New York: Wiley, 2010).
44. C.W. Chen, *Magnetism and Metallurgy of Soft Magnetic Materials* (Amsterdam, the Netherlands: North Holland, 1977).
45. O. Dahl, F.E. Pawlek, and J. Pfaffenberger, *Archiv Fur Eisenhüttenwesen* 9, 103 (1935).
46. J.B. Goodenough, *Phys. Rev.* 95, 917 (1954).
47. A. Mager, *Ann. Phys. Leipzig* 11, 15 (1952).
48. A. Mager, personal communication, 1988.
49. G. Bertotti, F. Fiorillo, and M. Pasquale, *J. Appl. Phys.* 69, 5930 (1991).
50. N. Gao, S.C. Wang, H.S. Ubhi, and M.J. Starink, *J. Mater. Sci.* 40, 4971 (2005).
51. D.L. Rodrigues, J.R.F. Silveira, and F.J.G. Landgraf, *IEEE Trans. Magn.* 47, 2179 (2011).
52. S.S.F. Dafé, S.C. Paolinelli, and A.B. Costa, *J. Magn. Magn. Mater.* 323, 3234 (2011).
53. B. De Boer and J. Wieting, *Scripta Mater.* 37, 753 (1997).
54. J.-T. Park and J.A. Szpunar, *Acta Mater.* 51, 3037 (2003).
55. L. Kestens, J.J. Jonas, P. Van Houtte, and E. Aernoudt, *Metall. Mater. Trans. A* 27, 2347 (1996).
56. T. Yonamine and F.J.G. Landgraf, *J. Magn. Magn. Mater.* 272, e565 (2004).
57. L. Kestens and S. Jacobs, *Texture Stress Microstruct.* 2008, Article ID 173083 (9 pages) (2008). doi:10.1155/2008/173083.

58. C.K. Hou and C.C. Liao, *ISIJ Int.* 48, 531 (2008).
59. V. Permiakov, L. Dupre, D. Makaveev, and J. Melkebeek, *J. Appl. Phys.* 91, 7854 (2002).
60. A. Martínez-de-Guerenu, K. Gurruchaga, and F. Arizti, *J. Magn. Magn. Mater.* 316, e842 (2007).
61. D.L. Rodrigues, J.R.F. Silveira, G.J.L. Gerhardt, F.P. Missell, F.J.G. Landgraf, R. Machado, and M.F. de Campos, *IEEE Trans. Magn.* 48, 1425 (2012).
62. H. Kronmuller, *Int. J. Nondestr. Test.* 3, 315 (1972).
63. A.S. Keh and S. Weissman, *Electron Microscopy and Strength of Crystals* (New York: Wiley Interscience, 1963), pp. 231–300.
64. A. Pulnikov, V. Permiakov, R. Petrov, J. Gyselinck, G. Langelaan, H. Wisselink, L. Dupre, Y. Houbaert, and J. Melkebeek, *J. Magn. Magn. Mater.* 272, 2303 (2004).
65. M.J. Sablik, F.J.G. Landgraf, R. Magnabosco, M. Fukuhara, M.F. de Campos, R. Machado, and F.P. Missell, *J. Magn. Magn. Mater.* 304, 155 (2006).
66. V.E. Iordache, E. Hug, and N. Buiron, *Mater. Sci. Eng. A* 359, 62 (2003).
67. C.K. Hou, *IEEE Trans. Magn.* 30, 212 (1994).
68. F.J.G. Landgraf and M. Emura, *J. Magn. Magn. Mater.* 242, 152 (2002).
69. R. Baiotto, G. Gerhardt, M. Fukuhara, T. Yonamine, and F.P. Missell, *IEEE Trans. Magn.* 46, 294 (2010).
70. T. Ros-Yañes, Y. Houbert, and V. Gomez-Rodrigues, *J. Appl. Phys.* 91, 7857 (2002).
71. C.A. Hernandez-Aramburo and A.C. Smith, *IEEE Trans. Magn.* 39, 3527 (2003).
72. J.G. Zhu and V.S. Ramsden, *IEEE Trans. Magn.* 34, 2234 (1998).
73. Y. Guo, J.G. Zhu, J. Zhong, H. Lu, and J.X. Jin, *IEEE Trans. Magn.* 44, 279 (2008).
74. J. Sagarduy and A.J. Moses, *J. Magn. Magn. Mater.* 320, e614 (2008).
75. M.S. Lancarotte and A.A. Penteado Jr, *IEEE Trans. Energ. Conv.* 16, 174 (2001).
76. G. Bertotti, *Hysteresis in Magnetism for Physicists, Material Scientists and Engineers* (New York: Academic Press, 1998).